

Tunable Single- and Multiphoton Bundles in Cavity-Coupled Atomic Arrays

Geng Zhao,^{1,*} Yun Chen,^{1,*} Jiayuang Zhang,¹ Jing Tang,^{2,3,†} and Yuangang Deng^{1,‡}

¹Guangdong Provincial Key Laboratory of Quantum Metrology and Sensing & School of Physics and Astronomy, Sun Yat-Sen University, Zhuhai 519082, China

²School of Physics and Optoelectronic Engineering, Guangdong University of Technology, Guangzhou 510006, China

³Guangdong Provincial Key Laboratory of Sensing Physics and System Integration Applications, Guangdong University of Technology, Guangzhou, 510006, China

(Dated: December 2, 2025)

We propose an experimentally accessible scheme for realizing tunable nonclassical light in cavity-coupled reconfigurable atomic arrays. By coherently controlling the collective interference phase, the system switches from single-photon blockade to high-purity multiphoton bundle emission, unveiling a hierarchical structure of photon correlations dictated by atom-number parity and cavity detuning. The scaling of photon population identifies the transition between superradiant and subradiant regimes, while parity- and phase-dependent spin correlations elucidate the microscopic interference processes enabling coherent multiphoton generation. This work establishes a unified framework connecting cooperative atomic interactions to controllable nonclassical photon statistics and introduces a distinct interference-enabled mechanism that provides a practical route toward high-fidelity multiphoton sources in scalable cavity QEDs.

Introduction.—The realization of tunable light-matter interfaces lies at the heart of quantum science, providing essential building blocks for quantum information and precision metrology [1–5]. Cavity quantum electrodynamics (QEDs) offers a natural platform for exploring strongly coupled systems, enabling engineering highly correlated nonclassical states with tailored coherence properties. Significant progress has been achieved in developing strongly nonlinearities for realizing photon blockade [6–13] and multiphoton bundle states [14–17], establishing a pathway toward scalable quantum networks [18–20] and nondestructive quantum measurements [21–23]. Concurrently, optical tweezer arrays of neutral atoms and polar molecules have emerged as a versatile platform combining single-particle addressability, long coherence times, and programmable long-range interactions [24–28]. These arrays have enabled advances in quantum simulation of strongly correlated many-body physics [29–32], scalable quantum computing [33–36], deterministic entanglement [37–40], and precision quantum sensing [41–43].

Integrating such atomic arrays into high-finesse optical cavities introduces cavity-mediated infinite-range interactions [44–49], opening new avenues to explore nonequilibrium quantum phases of light and matter. Recent experiments with cavity-coupled atom arrays have revealed cooperative radiation phenomena, including superradiance and subradiance [50–54], arising from phase-dependent interference determined by the spatial arrangement of emitters. Controllable switching between these regimes provides an unprecedented handle to engineer collective emission, decoherence, and photon correlations [55]. Despite these advances, the emergence of nonclassical multiphoton bundle states across radiance transitions remains largely unexplored. Establishing a

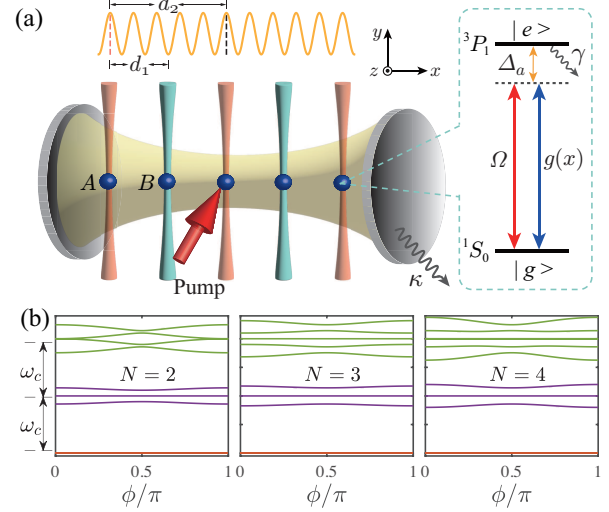


Figure 1. (a) Schematic of cavity-coupled reconfigurable atomic array, highlighting dipole-forbidden $^1S_0 \leftrightarrow ^3P_1$ transition of ^{88}Sr . (b) Phase ϕ dependence of anharmonic energy spectrum for different atom numbers N .

microscopic connection between collective atomic correlations and photon-number hierarchy is crucial for bridging cooperative atom-light physics and nonclassical photon generation.

In this Letter, we present an experimental scheme to achieve controllable nonclassical light emission in cavity-coupled atomic arrays. By tuning the collective interference phase between neighboring atoms, the system undergoes a transition from superradiant to subradiant regimes, accompanied by the emergence of high-quality multiphoton bundle state enabled by interference-suppressed single-photon excitation. We show that the scaling of photon population with atom number directly

reflects the collective radiance transition, while parity- and phase-dependent spin correlations reveal the microscopic origin of bunching multiphoton generation. In contrast to recent studies focusing on collective emission in the vacuum-Rabi splitting or far-dispersive regimes [50–54], our study identifies a radiance-controlled quantum switch between single-photon and multiphoton bundle sources operating in the atom-cavity resonant regime. These results establish a unified framework linking collective light-matter correlations to nonclassical photon statistics. Remarkably, unlike previously explored routes to bundle state—such as Mollow physics [14], deterministic parametric down-conversion [56], n-phonon resonance processes [57], and parity-symmetry-protected multiphoton process [15], our cavity-coupled reconfigurable atom arrays provide a practical route toward on-demand multiphoton emitters for quantum technologies and precision metrology [58].

Model.—We consider atom arrays assembled with an one-dimensional optical tweezer array placed inside a high-finesse Fabry-Pérot cavity [Fig. 1(a)] [50, 51]. As a representative system, we focus on alkaline-earth atoms such as ^{88}Sr , whose positions can be precisely controlled [59]. The relevant optical transition couples the ground state of singlet $^1S_0 = |g\rangle$ to long-lived excited state of triplet $^3P_1 = |e\rangle$, interacting with cavity mode along x with single-atom-cavity coupling g and a transverse pump along y with Rabi frequency Ω . Owing to its dipole-forbidden nature, this transition features a narrow linewidth, with a spontaneous decay rate $\gamma = (2\pi)7.5$ kHz at $\lambda = 689$ nm [59]. Distinct from uniform arrays, the setup implements a reconfigurable two-sublattice geometry with tunable lattice constants d_1 and d_2 . The relative phase $\phi = kd_1$ (with wave vector $k = 2\pi/\lambda$) controls constructive or destructive interference, while odd-site atoms are prepared at integer-wavelength separations ($d_2 = 5\lambda$). By tuning d_1 , interference pathways can be programmed, enabling the generation of nonclassical photon states. For $N \leq 60$ atoms, the array length (≤ 103 μm) remains well within the cavity Rayleigh range (~ 1 mm), ensuring uniform coupling. This reconfigurable architecture offers a versatile platform for engineering controllable quantum sources spanning single-photon to multiphoton emission.

For an array of N spatially fixed two-level atoms, Rayleigh scattering from pump field into single-mode cavity can be mapped onto an effective two-component Tavis-Cummings model (TCM)

$$\hat{\mathcal{H}} = \Delta_c \hat{a}^\dagger \hat{a} + \Delta_a (\hat{J}_A^z + \hat{J}_B^z) + \Omega (\hat{J}_A^x + \hat{J}_B^x) + g \hat{a}^\dagger (\hat{J}_A^- + \cos \phi \hat{J}_B^-) + g \hat{a} (\hat{J}_A^+ + \cos \phi \hat{J}_B^+), \quad (1)$$

where \hat{a} is the cavity annihilation operator, Δ_c and Δ_a are the cavity- and atom-pump detunings, respectively. The collective spin operators $\hat{J}_{A,B}^{x,y,z} = \frac{1}{2} \sum_j^{N_{A,B}} \hat{\sigma}_j^{x,y,z}$ describe atoms in sublattices A and B , with $\hat{J}_{A,B}^\pm =$

$\hat{J}_{A,B}^x \pm i \hat{J}_{A,B}^y$, $N_{A(B)}$ being atom number in each sublattice, and $\hat{\sigma}^{x,y,z}$ being Pauli matrices. The light-matter interaction encodes phase-dependent coupling between cavity and sublattices, enabling interference-controlled cavity emission. Notably, non-interacting neutral atoms at different sites are coupled by the infinite-range cavity via Stokes processes with a photon annihilation accompanied by atomic excitation. Neglecting the weak transverse drive ($\Omega = 0$), the Hamiltonian (1) exhibits a continuous $U(1)$ symmetry generated by $\mathcal{R}_\theta = \exp(i\theta \hat{N}_e)$, with $\hat{N}_e = \hat{a}^\dagger \hat{a} + \hat{J}_A^z + \hat{J}_B^z$ the total excitation number. This symmetry commutes with the Hamiltonian, $[\mathcal{R}_\theta, \hat{\mathcal{H}}] = 0$, and its spontaneous breaking signals the optical switching from normal to superradiant phase [60].

Taking into account all dissipations, nonclassical photon emission is captured by solving the master equation

$$\frac{d\rho}{dt} = -i[\hat{\mathcal{H}}, \rho] + \kappa \mathcal{D}[\hat{a}]\rho + \frac{\gamma}{N_A} \mathcal{D}[\hat{J}_A^-]\rho + \frac{\gamma}{N_B} \mathcal{D}[\hat{J}_B^-]\rho, \quad (2)$$

where ρ is the density matrix of cavity-coupled atomic arrays, $\mathcal{D}[\hat{o}]\rho = \hat{o}\rho\hat{o}^\dagger - (\hat{o}^\dagger\hat{o}\rho + \rho\hat{o}^\dagger\hat{o})/2$ denotes standard Lindblad-type dissipation, and $\kappa = (2\pi)75$ kHz is the cavity decay rate [61, 62]. In contrast to alkaline-metal atom arrays with $\gamma/\kappa \gg 1$, the small ratio $\gamma/\kappa = 0.1$ is crucial for realizing high-fidelity multiphoton-bundle emission. In numerical simulations, we focus on atom-photon resonance, $\Delta_c = \Delta_a = \Delta$, single atom-cavity coupling $g/\kappa = 10$, and Rabi frequency $\Omega/\kappa = 0.2$.

To explore the quantum statistics, we introduce the generalized k th-order correlation function [63]

$$g_n^{(k)}(\tau_1, \dots, \tau_k) = \frac{\langle \prod_{i=1}^k [\hat{a}^\dagger(\tau_i)]^n \prod_{i=1}^k [\hat{a}(\tau_i)]^n \rangle}{\prod_{i=1}^k \langle [\hat{a}^\dagger(\tau_i)]^n [\hat{a}(\tau_i)]^n \rangle},$$

with $\tau_1 \leq \dots \leq \tau_k$. This function captures nonclassical emission ranging from isolated photons to n -photon bundles. Explicitly, $g_1^{(k)}$ reduces to the conventional k th-order correlation function for isolated photons. Single photon blockade is identified by $g_1^{(2)}(0) < 1$ and $g_1^{(2)}(0) < g_1^{(2)}(\tau)$, which indicates sub-Poissonian statistics and photon antibunching, respectively. By contrast, the criteria for n -photon bundle emission is $g_1^{(2)}(0) > g_1^{(2)}(\tau)$ and $g_n^{(2)}(0) < g_n^{(2)}(\tau)$, ensuring photon bunching within each bundle and antibunching between separated bundles [14, 56, 57].

Energy spectrum.—To reveal the mechanism of nonclassical photon emission, we first analyze the energy spectrum of cavity-coupled reconfigurable atomic array by diagonalizing the Hamiltonian (1). In the single-excitation subspace, the eigenenergies of three branches satisfy: $E_{1,\pm} = \Delta \pm g\sqrt{(N_A + N_B \cos^2 \phi)}$ and $E_{1,0} = \Delta$, with corresponding eigenstates

$$\begin{aligned} |\Psi_{1,\pm}\rangle &= \frac{1}{\sqrt{2}}[|1,0\rangle \pm (\beta_A|0,1_A\rangle + \beta_B|0,1_B\rangle)], \\ |\Psi_{1,0}\rangle &= -\beta_B|0,1_A\rangle + \beta_A|0,1_B\rangle, \end{aligned} \quad (3)$$

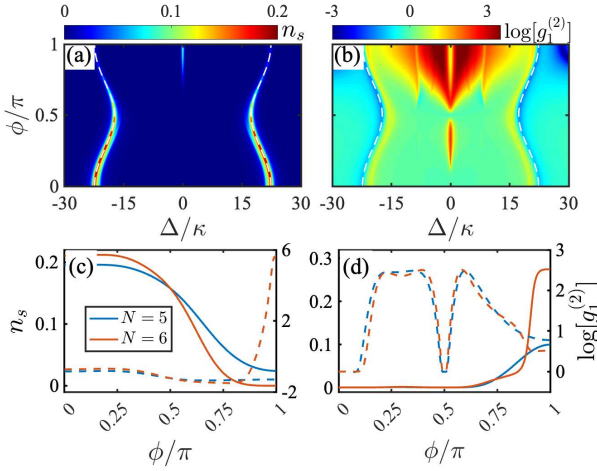


Figure 2. Distributions of (a) n_s and (b) $g_1^{(2)}(0)$ on the $\Delta - \phi$ plane for $N = 5$. The white dashed curves indicate the analytic dressed-state splitting at $\Delta = \Delta_{1,\pm}$. The phase ϕ dependence of n_s (solid line) and $g_1^{(2)}(0)$ (dashed line) for (c) $\Delta = |\Delta_{1,\pm}|$ and (d) $\Delta = 0$ at $N = 5$ and 6 , respectively. Color shading encodes the magnitude of n_s and $g_1^{(2)}(0)$.

where $|n, 0\rangle = |n, -\frac{N_A}{2}, -\frac{N_B}{2}\rangle$ with n being the photon number, $|n-1, 1_A\rangle = |n-1, 1, 1-\frac{N_A}{2}, -\frac{N_B}{2}\rangle$, and $|n-1, 1_B\rangle = |n-1, -\frac{N_A}{2}, 1, -\frac{N_B}{2}\rangle$ are introduced by shorthand notations. Here $\beta_A = \sqrt{N_A}/\sqrt{N_A + N_B \cos^2 \phi}$ and $\beta_B = \sqrt{N_B \cos \phi}/\sqrt{N_A + N_B \cos^2 \phi}$.

For $\phi = 0$, the spectrum contains two bright polaritons $|\Psi_{1,\pm}\rangle$ and one dark state $|\Psi_{1,0}\rangle$, corresponding to symmetric and anti-symmetric superpositions of A - and B -sublattice excitations. At $\phi = \pi$, this symmetry is reversed, while for arbitrary ϕ , the dark state persists with vanishing photon number at the single excitation subspace. Remarkably, even in weak-drive regime $\Omega/g \ll 1$, photon emission still occurs through the middle branch ($\Delta = 0$), indicating that multiphoton processes beyond the single-excitation manifold must be involved.

To reveal this mechanism, we calculate the full multiphoton spectrum, as detailed in Supplementary Materials [64]. For two atoms, the analytic n -photon dressed states associated with the middle branch at $\phi = \pi$ take the form ($n \geq 2$)

$$\begin{aligned} |\Psi_{n,0+}\rangle &= \frac{1}{\sqrt{2}}(|n-1, 1_A\rangle + |n-1, 1_B\rangle), \\ |\Psi_{n,0-}\rangle &= \frac{1}{\sqrt{2}}(|n, 0\rangle + |n-2, 2\rangle), \end{aligned} \quad (4)$$

with $|n-2, 2\rangle = |n-2, 1-\frac{N_A}{2}, 1-\frac{N_B}{2}\rangle$. Crucially, both $|\Psi_{n,0\pm}\rangle$ are symmetric across sublattices and remain degenerate at zero energy enabling multiphoton emission via destructive interference completely suppressing single-photon excitation. In particular, two-photon bundle emission arises from super-Rabi oscillations of $|2, 0\rangle \leftrightarrow |0, 2\rangle$, and analogous multiphoton super-Rabi

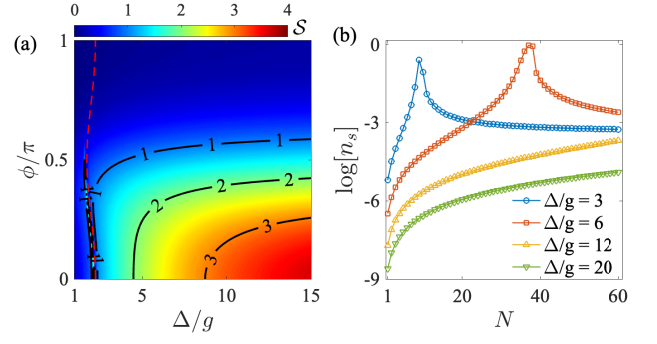


Figure 3. (a) S as functions of Δ and ϕ for $N = 5$. Solid lines are contour lines and the white dashed line shows vacuum Rabi splitting Δ_{1+} at blue sideband. (b) n_s versus N for $\phi = 0$ and $\Delta/g = 3, 6, 12$, and 20 . The black dashed line serves as a guide for $n_s \sim N^2$.

processes persist for $N \geq 3$. In contrast to earlier studies where destructive interference suppressed emission at $\phi = \pi$ [51], here the symmetric n th-order dressed states dominate when atoms rather than the cavity are directly driven, giving rise to nonclassical multiphoton emission. Notably, the middle-branch bundle emission is entirely absent for $\phi = 0$, consistent with quantum mechanical picture of collective scattering in cavity-coupled atom arrays [64].

Figure 1(b) illustrates ϕ -dependent anharmonic energy spectrum for different total atom numbers N . In the single-excitation manifold, three helicity branches consistently appear, in agreement with the analytic expressions in Eq. (3). Beyond this regime, the doubly excited spectrum becomes increasingly structured: it exhibits four, five, and six (including two degenerate) helicity branches for $N = 2$, $N = 3$, and $N \geq 4$, respectively. Strikingly, both single- and multiphoton excitations remain resonant for middle helicity at $\Delta = 0$, thereby opening a robust channel for generating multiphoton states that manifest as nonclassical photon bunching.

Subradiance to superradiance.—Figures 2(a) and 2(b) display the steady-state photon number n_s and second-order correlation function $g_1^{(2)}(0)$ as functions of detuning Δ and phase ϕ for $N = 5$. The dominant photon emission appears at the single-photon resonances $\Delta_{1\pm} = \pm g\sqrt{N_A + N_B \cos^2 \phi}$, which correspond to the bright polariton states $|\Psi_{1,\pm}\rangle$. These phase-dependent splittings $\Delta_{1\pm}$ represent an effective vacuum Rabi splitting, consistent with recent observations in cavity-coupled atomic arrays [51], and exhibit strong sensitivity to both N and ϕ . As shown in Fig. 2(c), photon number displays a pronounced contrast between constructive ($\phi = 0$) and destructive ($\phi = \pi$) interference, signaling the superradiant to subradiant transition.

At red and blue sidebands, superradiant emission exhibits photon blockade characterized by $g_1^{(2)}(0) < 1$. No-

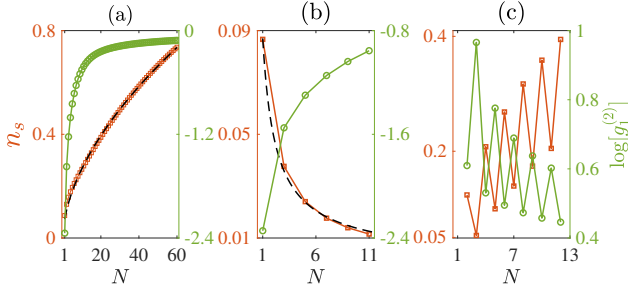


Figure 4. N dependence of n_s (red lines) and $g_1^{(2)}$ (green lines) for (a) $\phi = 0$ and (b) $\phi = \pi$ at $\Delta = |\Delta_{1\pm}|$, and (c) $[\phi, \Delta] = [\pi, 0]$, respectively. The dashed lines indicate power-law fits: $n_s = 0.07N^{0.56}$ in (a) and $n_s = 0.09N^{-0.8}$ in (b).

tably, the blockade strength is not monotonic in ϕ : the highest single-photon purity emerges for phase satisfying $\phi/\pi > 0.5$. Furthermore, the optimal phase depends sensitively on both parity and magnitude of N [64], revealing the subtle influence of array symmetry on the radiative response. In contrast, at the middle branch ($\Delta = 0$), the multiphoton dressed states with different excitation numbers n become simultaneously resonant [see Eq. (4)]. Consequently, the cavity output exhibits strong bunching with $g_1^{(2)}(0) > 1$, while n_s increases monotonically with ϕ [Fig. 2(d)]. Remarkably, $n_s(\Delta = 0, \phi = \pi)$ will reach a peak, regardless of whether N is even or odd, in sharp contrast to the bright sideband branches at $\Delta = |\Delta_{1\pm}|$. By symmetry, $n_s(\Delta = 0, \phi = 0)$ vanishes, since middle-branch state is antisymmetric at $\phi = 0$ but becomes symmetric at $\phi/\pi = 1$ with respect to two sublattices.

To proceed further, we study the steady-state photon emission scales with total atom number N in cavity-coupled reconfigurable arrays. Within the semiclassical treatment, the steady-state cavity population is

$$n_s = \left| \frac{g\Omega(N_A + N_B \cos \phi)}{\Delta(\Delta - i\kappa) - g^2(N_A + N_B \cos^2 \phi)} \right|^2. \quad (5)$$

At single-photon resonance $\Delta = \Delta_{1\pm}$, we obtain $n_s = N\Omega^2/\kappa^2$ for $\phi = 0$, revealing linear N scaling of bright states $|\Psi_{1,\pm}\rangle$. By contrast, photon emission shows a strong parity effect at $\phi = \pi$: for even N destructive interference completely suppresses cavity emission ($n_s = 0$), whereas for odd N we obtain $n_s = \Omega^2/(N\kappa^2)$, exhibiting an inverse $1/N$ scaling. For middle branch at $\Delta = 0$ and $\phi = \pi$, the parity dependence persists: $n_s = \Omega^2/(gN)^2$ for even N , while it vanishes identically for odd N . In the dispersive regime $\Delta/g \gg 1$, the photon number saturates to $n_s \sim (g\Omega/\Delta)^2$ for odd N at $\phi = \pi$, while for $\phi = 0$ it recovers the parity-independent superradiant scaling $n_s \sim (g\Omega N/\Delta)^2$. These results stem from mean-field analysis that neglects quantum fluctuations and correlations. The exact scaling behavior requires solving full master equation [Eq. (2)].

To characterize the subradiance-superradiance quantum phase transition, we introduce the order parameter

$\mathcal{S} = n_s(N, \Delta, \phi)/[Nn_s(1, \Delta_s, \phi)]$ with $\Delta_s = g + \Delta - \Delta_{1\pm}$, such that $\mathcal{S} > 1$ (< 1) signals superradiance (subradiance). Clearly, $n_s(1, \Delta_s, \phi)$ also reaches its maximum at $\Delta = \Delta_{1\pm}$ for $\phi = \pi$ and arbitrary N . Fig. 3(a) shows the distribution of \mathcal{S} on the $\Delta - \phi$ parameter plane. Due to photon blockade, the cavity always remains subradiant for $\Delta < \Delta_{1,+}$. Interestingly, the system undergoes a transition from subradiance to superradiance as Δ increases when $\phi/\pi < 0.5$. In particular, we find $\mathcal{S} > 3$ in the regime $\Delta/g \gg 1$ at small ϕ , demonstrating enhanced superradiance. Conversely, even at large detuning, increasing ϕ drives a superradiance-to-subradiance transition due to destructive interference.

To further explore scaling, Fig. 3(b) shows n_s versus N at $\phi = 0$ for different Δ . Notably, n_s increases rapidly with N and saturates to $N = (\Delta_{1\pm}/g)^2$ at single-photon resonance. For $N > (\Delta_{1\pm}/g)^2$, n_s decreases monotonically, contrasting with the scaling $n_s \propto N^2$ predicted by Eq. (5). For $\Delta/g \gg 1$, we find that the steady-state photon number follows $n_s \sim N^{2.22}$ ($N^{2.07}$) for $\Delta/g = 12$ (20). Thus, the quadratic N^2 scaling is recovered only in the strict far-dispersive limit, where mean-field description captures collective enhancement while neglecting quantum fluctuations [65–67].

Figures 4(a) and 4(b) show n_s and second-order correlation function $g_1^{(2)}(0)$ as a function of N at $\Delta = |\Delta_{1\pm}|$ for different ϕ . We find power-law scaling $n_s \sim N^{0.56}$ for $\phi = 0$ and $n_s \sim N^{-0.8}$ for $\phi = \pi$. In both case, the single-photon purity decreases monotonically as N increases. In the thermodynamic limit ($N \sim \infty$) and $\phi = 0$, cavity field evolves from single-photon state into coherent state with $g_1^{(2)}(0)$ to 1, signaling a quantum-to-classical transition in which photon blockade is gradually destroyed. A striking feature appears at $\phi = \pi$, where photon emission exhibits a pronounced parity dependence on N . For even N , destructive interference suppresses n_s entirely. This corresponds to antisymmetric bright states $|\Psi_{1,\pm}\rangle$ in Eq. (3). For odd N , the imbalance $N_A - N_B = 1$ breaks the symmetry, allowing residual photon emission. Remarkably, in both cases the scaling laws $n_s \sim N^{0.56}$ ($\phi = 0$) and $n_s \sim N^{-0.8}$ ($\phi = \pi$) deviate strongly from mean-field prediction of Eq. (5), demonstrating the crucial role of quantum fluctuations in collective cavity scattering. Our results uncover a hierarchy of scaling laws from suppressed $1/N$ subradiance to enhanced N^2 superradiance controlled by phase-dependent interference.

In Fig. 4(c), we show n_s and $g_1^{(2)}(0)$ at $\Delta = 0$ and $\phi = \pi$. Although parity dependence persists, n_s remains finite even for even N , in contrast to perfect destructive interference that appears at sidebands. Strikingly, the middle branch exhibits strong photon bunching ($g_1^{(2)}(0) \gg 1$), suggesting a high-quality source of multiphoton states. We emphasize that photon emission with bunched statistics at middle branch yet studied in experiments [50, 51]. Unlike superradiant coherent emis-

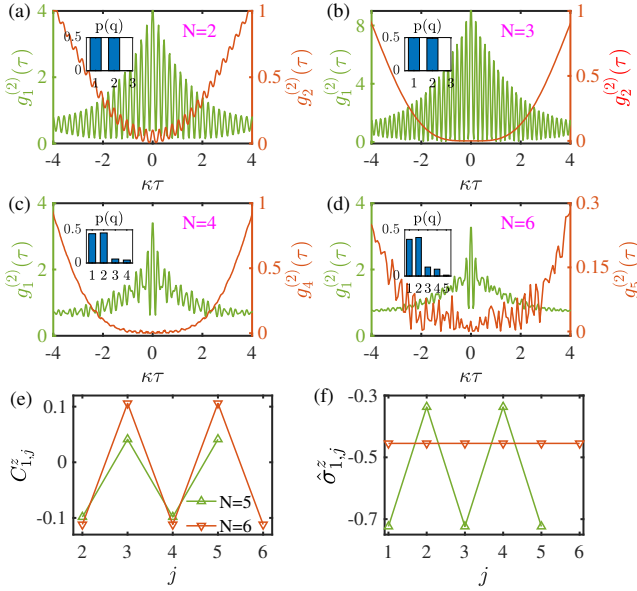


Figure 5. (a)-(d) Time interval τ dependence of $g_1^{(2)}(\tau)$ (solid lines) and $g_n^{(2)}(\tau)$ (dashed lines) for $N = 2, 3, 4$, and 6 , respectively. The inset displays the steady-state photon distribution $p(q)$. Spatial profiles of (e) correlations $C_{1,j}^z$ and (f) spin magnetism $\langle \hat{\sigma}_j^z \rangle$ as function of lattice site j for different N . The other parameters are $\phi = \pi$ and $\Delta = 0$.

sion observed in the far-dispersive regime [50], our results reveal a transition from antibunched single-photon to bunched multiphoton emission under in atom-cavity resonance. Moreover, generating multiphoton emission on the middle branch requires pump atoms directly, rather than driven the cavity field [51]. We also confirm that $n_s(\Delta = 0)$ vanishes without external drive ($\Omega = 0$). Finally, a small ratio γ/κ is also essential for realizing nonclassical bunched emission in cavity-coupled alkaline-earth atom arrays.

N-photon bundle emission.—To demonstrate nonclassical emission, we calculate interval dependence of correlation functions $g_1^{(2)}(\tau)$ and $g_n^{(2)}(\tau)$ for characterizing n -photon bundle generation. For $N = 2$ and 3 [Fig. 5(a) and Fig. 5(b)], two-photon bundle emerge at middle branch ($\Delta = 0$) with $\phi = \pi$, satisfying $g_1^{(2)}(0) > g_1^{(2)}(\tau)$ and $g_2^{(2)}(0) < g_2^{(2)}(\tau)$, signatures of photon bunching within a bundle and antibunching for separated bundles [14, 56, 57]. The associated correlation lifetimes significantly exceed $1/\kappa$, enabled by the long-lived alkaline-earth atoms with $\gamma/\kappa \ll 1$. For $N = 4$ [Fig. 5(c)], we observe a clearly resolved four-photon bundle, again exhibiting the characteristic correlation signatures $g_1^{(2)}(0) > g_1^{(2)}(\tau)$ and $g_4^{(2)}(0) < g_4^{(2)}(\tau)$. Remarkably, large N further facilitates higher-order bundles [Fig. 5(d)], with accessible order n controlled by pump strength Ω and atom-cavity coupling g . Importantly, photon population remains sizable ($n_s > 10^{-1}$) and increases substantially with N [Fig. 4(c)].

To further quantify bundle emission, we evaluate steady-state photon-number distribution $p(q) = \text{tr}(q|q\rangle\langle q|\rho)/n_s$, which characterize the weight of q -photon states among total emitted photons. For n -photon bundle, $p(q)$ rapidly decreases and essentially vanishes for $q > n$, providing clear evidence of strong $(n + 1)$ -photon blockade. Unlike Mollow emission in far-dispersive regime [14], our cavity-coupled reconfigurable atom arrays offer a practical route to high-quality multiphoton sources by completely suppressing single-photon excitation via interference, without requiring the strong-coupling limit and while mitigating detrimental heating or decoherence associated with a strong pump field.

To elucidate microscopic origin of photon emission, we examine connected spin correlations $C_{i,j}^z = \langle \hat{\sigma}_i^z \hat{\sigma}_j^z \rangle - \langle \hat{\sigma}_i^z \rangle \langle \hat{\sigma}_j^z \rangle$ across all spin pairs (i, j) [53, 68]. In Fig. 5(e) and 5(f), we plot $C_{1,j}^z$ and spin magnetism $\langle \hat{\sigma}_j^z \rangle$ as a function of lattice site j . A pronounced alternation of positive (negative) correlations on even (odd) sites is observed, reflecting the intrinsic the configuration of AB sublattice. Notably, the correlation profiles $C_{1,j}^z$ is highly sensitive to the parity of N . In particular, even N yields strong long-range order ($|C_{1,j}^z| \approx 0.1$), favorable for multiphoton bundle formation. The alternating sign of $C_{1,j}^z$ reveals a π -phase shift between neighboring atoms arising from their half-integer wavelength separation. Moreover, the distance-independent amplitude of $C_{1,j}^z$ directly evidences the infinite-range nature of cavity-mediated interactions. Consistently, the spin magnetization $\langle \hat{\sigma}_j^z \rangle \approx -0.45$ remains homogeneous for even N , whereas odd N exhibits a clear staggered magnetization.

In contrast, single-photon emission at $\Delta = \Delta_{1\pm}$ and $\phi = 0$ shows correlation collapsing to $C_{1,j}^z \approx -0.01$ and nearly fully polarized spins $\langle \hat{\sigma}_j^z \rangle < -0.9$. This behavior is consistent with photon blockade: emission of the first photon suppresses subsequent excitations, producing high-purity single-photon states with vanishing inter-atomic correlations. Taken together, these results demonstrate that spin correlations in cavity-coupled arrays provide a powerful diagnostic for distinguishing emission regimes, ranging from pronounced single-photon blockade to the emergence of collective n -photon bundle.

Conclusion.—We have proposed a realistic and experimentally accessible scheme to realize tunable transitions between superradiant and subradiant emission in cavity-coupled atomic arrays. By systematically analyzing the power-law scaling of photon population with array size, we uncover that the hierarchy of photon correlations provides a direct signature of collective radiance transitions. The interplay of collective phase interference and atomic parity enables deterministic control over nonlinear quantum emission—from single-photon blockade to collective n -photon bundle generation. The observed parity- and phase-dependent spin correlations and magnetization provides a microscopic diagnostic for distinguishing distinct cooperative emission regimes. Our work estab-

lishes a new perspective on the many-body mechanisms underlying nonclassical light generation and presents a feasible route for engineering tunable quantum switch between high-quality single-photon to multiphoton sources in scalable cavity QEDs. Beyond atomic platforms, the proposed mechanism can be readily extended to cavity-coupled reconfigurable polar molecule arrays, where long-range dipolar interactions may drive novel superradiance and strongly correlated quantum emission [69]. These results open promising directions for engineering hybrid quantum interfaces that exploit cooperative light-matter physics for quantum information processing and precision metrology [38, 39].

Acknowledgments.—This work was supported by the National Natural Science Foundation of China (Grant No.12374365, Grant No. 12274473, and Grant No. 12135018) and Guangdong University of Technology SPOE Seed Foundation (SF2024111504).

* These authors contributed equally to this work.

† jingtang@gdut.edu.cn

‡ dengyg3@mail.sysu.edu.cn

- [1] D. E. Chang, J. S. Douglas, A. González-Tudela, C.-L. Hung, and H. J. Kimble, Colloquium: Quantum matter built from nanoscopic lattices of atoms and photons, *Rev. Mod. Phys.* **90**, 031002 (2018).
- [2] M. G. Kozlov, M. S. Safronova, J. R. Crespo López-Urrutia, and P. O. Schmidt, Highly charged ions: Optical clocks and applications in fundamental physics, *Rev. Mod. Phys.* **90**, 045005 (2018).
- [3] Z. Li, S. Colombo, C. Shu, G. Velez, S. Pilatowsky-Cameo, R. Schmied, S. Choi, M. Lukin, E. Pedrozo-Peñañiel, and V. Vuletić, Improving metrology with quantum scrambling, *Science* **380**, 1381 (2023).
- [4] C. Hotter, H. Ritsch, and K. Gietka, Combining critical and quantum metrology, *Phys. Rev. Lett.* **132**, 060801 (2024).
- [5] Z. Zou, J. Gong, and W. Chen, Enhancing quantum metrology by quantum resonance dynamics, *Phys. Rev. Lett.* **134**, 230802 (2025).
- [6] K. M. Birnbaum, A. Boca, R. Miller, A. D. Boozer, T. E. Northup, and H. J. Kimble, Photon blockade in an optical cavity with one trapped atom, *Nature* **436**, 87 (2005).
- [7] T. Aoki, B. Dayan, E. Wilcut, W. P. Bowen, A. S. Parkins, T. Kippenberg, K. Vahala, and H. Kimble, Observation of strong coupling between one atom and a monolithic microresonator, *Nature* **443**, 671 (2006).
- [8] K. Srinivasan and O. Painter, Linear and nonlinear optical spectroscopy of a strongly coupled microdisk-quantum dot system, *Nature* **450**, 862 (2007).
- [9] B. Dayan, A. Parkins, T. Aoki, E. Ostby, K. Vahala, and H. Kimble, A photon turnstile dynamically regulated by one atom, *Science* **319**, 1062 (2008).
- [10] T. C. H. Liew and V. Savona, Single photons from coupled quantum modes, *Phys. Rev. Lett.* **104**, 183601 (2010).
- [11] C. Hamsen, K. N. Tolazzi, T. Wilk, and G. Rempe, Two-photon blockade in an atom-driven cavity qed system, *Phys. Rev. Lett.* **118**, 133604 (2017).
- [12] Y.-H. Zhou, T. Liu, Q.-P. Su, X.-Y. Zhang, Q.-C. Wu, D.-X. Chen, Z.-C. Shi, H. Z. Shen, and C.-P. Yang, Universal photon blockade, *Phys. Rev. Lett.* **134**, 183601 (2025).
- [13] Z.-G. Lu, Y. Wu, and X.-Y. Lü, Chiral interaction induced near-perfect photon blockade, *Phys. Rev. Lett.* **134**, 013602 (2025).
- [14] C. S. Muñoz, E. D. Valle, A. G. Tudela, K. Müller, and F. P. Laussy, Emitters of n-photon bundles, *Nat. Photonics* **8**, 550 (2014).
- [15] Q. Bin, Y. Wu, and X.-Y. Lü, Parity-symmetry-protected multiphoton bundle emission, *Phys. Rev. Lett.* **127**, 073602 (2021).
- [16] C. Liu, J.-F. Huang, and L. Tian, Deterministic generation of multi-photon bundles in a quantum rabi model, *Science China Physics, Mechanics & Astronomy* **66**, 220311 (2023).
- [17] Q. Bin, H. Jing, Y. Wu, F. Nori, and X.-Y. Lü, Non-reciprocal bundle emissions of quantum entangled pairs, *Phys. Rev. Lett.* **133**, 043601 (2024).
- [18] S. Ritter, C. Nölleke, C. Hahn, A. Reiserer, A. Neuzner, M. Uphoff, M. Mücke, E. Figueroa, J. Bochmann, and G. Rempe, An elementary quantum network of single atoms in optical cavities, *Nature* **484**, 195 (2012).
- [19] H. J. Kimble, The quantum internet, *Nature* **453**, 1023 (2008).
- [20] W. Redjem, Y. Zhiyenbayev, W. Qarony, V. Ivanov, C. Papapanos, W. Liu, K. Jhuria, Z. Al Balushi, S. Dhuey, A. Schwartzberg, *et al.*, All-silicon quantum light source by embedding an atomic emissive center in a nanophotonic cavity, *Nat. Commun.* **14**, 3321 (2023).
- [21] D. Niemietz, P. Farrera, S. Langenfeld, and G. Rempe, Nondestructive detection of photonic qubits, *Nature* **591**, 570 (2021).
- [22] L.-M. Duan and H. J. Kimble, Scalable photonic quantum computation through cavity-assisted interactions, *Phys. Rev. Lett.* **92**, 127902 (2004).
- [23] A. Reiserer, S. Ritter, and G. Rempe, Nondestructive detection of an optical photon, *Science* **342**, 1349 (2013).
- [24] S. Ebadi, T. T. Wang, H. Levine, A. Keesling, G. Semeghini, A. Omran, D. Bluvstein, R. Samajdar, H. Pichler, W. W. Ho, *et al.*, Quantum phases of matter on a 256-atom programmable quantum simulator, *Nature* **595**, 227 (2021).
- [25] I. Bloch, J. Dalibard, and Sylvain, Quantum simulations with ultracold quantum gases, *Nat. Phys.* **8**, 267 (2012).
- [26] D. Barredo, S. de Léséleuc, V. Lienhard, T. Lahaye, and A. Browaeys, An atom-by-atom assembler of defect-free arbitrary two-dimensional atomic arrays, *Science* **354**, 1021 (2016).
- [27] L. Anderegg, L. W. Cheuk, Y. Bao, S. Burchesky, W. Ketterle, K.-K. Ni, and J. M. Doyle, An optical tweezer array of ultracold molecules, *Science* **365**, 1156 (2019).
- [28] W. B. Cairncross, J. T. Zhang, L. R. B. Picard, Y. Yu, K. Wang, and K.-K. Ni, Assembly of a rovibrational ground state molecule in an optical tweezer, *Phys. Rev. Lett.* **126**, 123402 (2021).
- [29] H. Bernien, S. Schwartz, A. Keesling, H. Levine, A. Omran, H. Pichler, S. Choi, A. S. Zibrov, M. Endres, M. Greiner, *et al.*, Probing many-body dynamics on a 51-atom quantum simulator, *Nature* **551**, 579 (2017).
- [30] J. Zhang, G. Pagano, P. W. Hess, A. Kyprianidis, P. Becker, H. Kaplan, A. V. Gorshkov, Z.-X. Gong,

- and C. Monroe, Observation of a many-body dynamical phase transition with a 53-qubit quantum simulator, *Nature* **551**, 601 (2017).
- [31] S. De Léséleuc, V. Lienhard, P. Scholl, D. Barredo, S. Weber, N. Lang, H. P. Büchler, T. Lahaye, and A. Browaeys, Observation of a symmetry-protected topological phase of interacting bosons with rydberg atoms, *Science* **365**, 775 (2019).
- [32] Z. Yue, Y.-F. Mao, X. Liang, Z.-X. Hua, P. Ge, Y.-X. Chao, K. Li, C. Jia, M. K. Tey, Y. Xu, *et al.*, Observing structural disorder induced interacting topological phase in an atom array, *arXiv preprint arXiv:2505.06286* (2025).
- [33] D. DeMille, Quantum computation with trapped polar molecules, *Phys. Rev. Lett.* **88**, 067901 (2002).
- [34] A. Browaeys and T. Lahaye, Many-body physics with individually controlled rydberg atoms, *Nat. Phys.* **16**, 132 (2020).
- [35] A. M. Kaufman and K.-K. Ni, Quantum science with optical tweezer arrays of ultracold atoms and molecules, *Nat. Phys.* **17**, 1324 (2021).
- [36] Z. Z. Yan, B. M. Spar, M. L. Prichard, S. Chi, H.-T. Wei, E. Ibarra-García-Padilla, K. R. A. Hazzard, and W. S. Bakr, Two-dimensional programmable tweezer arrays of fermions, *Phys. Rev. Lett.* **129**, 123201 (2022).
- [37] T. Wilk, A. Gaëtan, C. Evellin, J. Wolters, Y. Miroshnychenko, P. Grangier, and A. Browaeys, Entanglement of two individual neutral atoms using rydberg blockade, *Phys. Rev. Lett.* **104**, 010502 (2010).
- [38] C. M. Holland, Y. Lu, and L. W. Cheuk, On-demand entanglement of molecules in a reconfigurable optical tweezer array, *Science* **382**, 1143 (2023).
- [39] Y. Bao, S. S. Yu, L. Anderegg, E. Chae, W. Ketterle, K.-K. Ni, and J. M. Doyle, Dipolar spin-exchange and entanglement between molecules in an optical tweezer array, *Science* **382**, 1138 (2023).
- [40] N. Schine, A. W. Young, W. J. Eckner, M. J. Martin, and A. M. Kaufman, Long-lived bell states in an array of optical clock qubits, *Nat. Phys.* **18**, 1067 (2022).
- [41] C. D. Marciniak, T. Feldker, I. Pogorelov, R. Kaubruegger, D. V. Vasilyev, R. van Bijnen, P. Schindler, P. Zoller, R. Blatt, and T. Monz, Optimal metrology with programmable quantum sensors, *Nature* **603**, 604 (2022).
- [42] R. Kaubruegger, P. Silvi, C. Kokail, R. van Bijnen, A. M. Rey, J. Ye, A. M. Kaufman, and P. Zoller, Variational spin-squeezing algorithms on programmable quantum sensors, *Phys. Rev. Lett.* **123**, 260505 (2019).
- [43] D. Schäffner, T. Schreiber, F. Lenz, M. Schlosser, and G. Birkel, Quantum sensing in tweezer arrays: Optical magnetometry on an individual-atom sensor grid, *PRX Quantum* **5**, 010311 (2024).
- [44] R. Reimann, W. Alt, T. Kampschulte, T. Macha, L. Ratschbacher, N. Thau, S. Yoon, and D. Meschede, Cavity-modified collective rayleigh scattering of two atoms, *Phys. Rev. Lett.* **114**, 023601 (2015).
- [45] S. Begley, M. Vogt, G. K. Gulati, H. Takahashi, and M. Keller, Optimized multi-ion cavity coupling, *Phys. Rev. Lett.* **116**, 223001 (2016).
- [46] S. Welte, B. Hacker, S. Daiss, S. Ritter, and G. Rempe, Cavity carving of atomic bell states, *Phys. Rev. Lett.* **118**, 210503 (2017).
- [47] B. Casabone, K. Friebe, B. Brandstätter, K. Schüppert, R. Blatt, and T. E. Northup, Enhanced quantum interface with collective ion-cavity coupling, *Phys. Rev. Lett.* **114**, 023602 (2015).
- [48] T. Dorđević, P. Samutpraphoot, P. L. Ocola, H. Bernien, B. Grinkemeyer, I. Dimitrova, V. Vuletić, and M. D. Lukin, Entanglement transport and a nanophotonic interface for atoms in optical tweezers, *Science* **373**, 1511 (2021).
- [49] E. Deist, J. A. Gerber, Y.-H. Lu, J. Zeiher, and D. M. Stamper-Kurn, Superresolution microscopy of optical fields using tweezer-trapped single atoms, *Phys. Rev. Lett.* **128**, 083201 (2022).
- [50] Z. Yan, J. Ho, Y.-H. Lu, S. J. Masson, A. Asenjo-Garcia, and D. M. Stamper-Kurn, Superradiant and subradiant cavity scattering by atom arrays, *Phys. Rev. Lett.* **131**, 253603 (2023).
- [51] Y. Liu, Z. Wang, P. Yang, Q. Wang, Q. Fan, S. Guan, G. Li, P. Zhang, and T. Zhang, Realization of strong coupling between deterministic single-atom arrays and a high-finesse miniature optical cavity, *Phys. Rev. Lett.* **130**, 173601 (2023).
- [52] S. J. Masson, I. Ferrier-Barbut, L. A. Orozco, A. Browaeys, and A. Asenjo-Garcia, Many-body signatures of collective decay in atomic chains, *Phys. Rev. Lett.* **125**, 263601 (2020).
- [53] T. O. Puel and T. Macrì, Confined meson excitations in rydberg-atom arrays coupled to a cavity field, *Phys. Rev. Lett.* **133**, 106901 (2024).
- [54] Y. Han, H. Li, and W. Yi, Interaction-enhanced superradiance of a rydberg-atom array, *Phys. Rev. Lett.* **133**, 243401 (2024).
- [55] J. Rui, D. Wei, A. Rubio-Abadal, S. Hollerith, J. Zeiher, D. M. Stamper-Kurn, C. Gross, and I. Bloch, A subradiant optical mirror formed by a single structured atomic layer, *Nature* **583**, 369 (2020).
- [56] Y. Chang, A. González-Tudela, C. Sánchez Muñoz, C. Navarrete-Benlloch, and T. Shi, Deterministic down-converter and continuous photon-pair source within the bad-cavity limit, *Phys. Rev. Lett.* **117**, 203602 (2016).
- [57] Y. Deng, T. Shi, and S. Yi, Motional n-phonon bundle states of a trapped atom with clock transitions photon (2021).
- [58] A. Neuzner, M. Körber, O. Morin, S. Ritter, and G. Rempe, Interference and dynamics of light from a distance-controlled atom pair in an optical cavity, *Nat. Photonics* **10**, 303 (2016).
- [59] M. N. Winchester, M. A. Norcia, J. R. K. Cline, and J. K. Thompson, Magnetically induced optical transparency on a forbidden transition in strontium for cavity-enhanced spectroscopy, *Phys. Rev. Lett.* **118**, 263601 (2017).
- [60] J. Tang and Y. Deng, Unveiling vacuum fluctuations and nonclassical states with cavity-enhanced tripartite interactions, *APL Photonics* **9** (2024).
- [61] M. L. Peters, G. Wang, D. C. Spierings, N. Drucker, B. Hu, M.-W. Chen, Y.-T. Chen, and V. Vuletić, Cavity-enabled real-time observation of individual atomic collisions, *Phys. Rev. Lett.* **135**, 093402 (2025).
- [62] P. Kongkhambut, J. Skulte, L. Mathey, J. G. Cosme, A. Hemmerich, and H. Keßler, Observation of a continuous time crystal, *Science* **377**, 670 (2022).
- [63] J. Tang and Y. Deng, Tunable multiphoton bundles emission in a kerr-type two-photon jaynes-cummings model, *Phys. Rev. Res.* **6**, 033247 (2024).
- [64] G. Zhao, Supplementary materials: Single to bundle photon emissions in cavity-coupled reconfigurable atom ar-

- rays, See Supplemental Material for detailed derivations (2025), appendix sections [Energy spectrum].
- [65] K. Baumann, C. Guerlin, F. Brennecke, and T. Esslinger, Dicke quantum phase transition with a superfluid gas in an optical cavity, [*Nature* **464**, 1301 \(2010\)](#).
 - [66] Y. Deng, J. Cheng, H. Jing, and S. Yi, Bose-einstein condensates with cavity-mediated spin-orbit coupling, [*Phys. Rev. Lett.* **112**, 143007 \(2014\)](#).
 - [67] Y. Deng and S. Yi, Self-ordered supersolid phase beyond dicke superradiance in a ring cavity, [*Phys. Rev. Res.* **5**, 013002 \(2023\)](#).
 - [68] G. Emperauger, M. Qiao, C. Chen, F. Caleca, S. Bocini, M. Bintz, G. Bornet, R. Martin, B. Gély, L. Klein, D. Barredo, S. Chatterjee, N. Yao, F. Mezzacapo, T. Lahaye, T. Roscilde, and A. Browaeys, [Tomonaga-luttinger liquid behavior in a rydberg-encoded spin chain](#) (2025), [arXiv:2501.08179 \[quant-ph\]](#).
 - [69] Y. Wang, S. Yi, and Y. Deng, Dark superradiance in cavity-coupled polar molecular bose-einstein condensates, [arXiv preprint arXiv:2504.18125 \(2025\)](#).